TITLE

Phosphatidylinositol Cycle Disruption is Central to Atypical Hemolytic-Uremic Syndrome Caused by Diacylglycerol Kinase Epsilon Deficiency

RUNNING TITLE

Low PIP_2 is central to *DGKE* aHUS

AUTHORS

Vincent So[1,2], Jing Wu[1], Alexis Traynor-Kaplan[3], Christopher Choy[4], Richard Epand[5], Roberto Botelho[4], Mathieu Lemaire[1,2,6,7]

AFFILIATIONS

1. Cell Biology Program, SickKids Research Institute, Toronto, CA
2. Department of Biochemistry, Faculty of Medicine, University of Toronto, Toronto, CA
3. Department of Medicine, Washington University School of Medicine, Seattle, USA
4. Department of Chemistry and Biology and Molecular Science Program, Ryerson University, Toronto, CA
5. Department of Biochemistry and Biomedical Sciences, McMaster University, Hamilton, CA
6. Institute of Medicine, Faculty of Medicine, University of Toronto, Toronto, CA
7. Division of Nephrology, The Hospital for Sick Children, Toronto, CA

KEY WORDS (6)

Diacylglycerol kinase epsilon, diacylglycerols, atypical hemolytic-uremic syndrome, phosphatidylinositols, inborn error of lipid metabolism, vascular endothelium

CORRESPONDING AUTHOR

Mathieu Lemaire, PGCRL building, SickKids Research Institute, Toronto, ON, M5G 0A4, Canada.

Email: mathieu.lemaire@sickkids.ca

Number of words, abstract: 228
Number of words, main text: 3,565
Number of figures: 5
Number of supplemental figures: 5

ABSTRACT

Background: Loss-of-function mutations in diacylglycerol kinase epsilon (*DGKE*) cause a rare form of atypical hemolytic-uremic syndrome (aHUS) for which there is no treatment besides kidney transplantation. Highly expressed in kidney endothelial cells, DGKE is a lipid kinase that phosphorylates diacylglycerol (DAG) to phosphatic acid (PA). Specifically, DGKE's preferred substrate is 38:4-DAG, that is DAG containing stearic acid (18:0) and arachidonic acid (20:4). DAG is produced when phosphatidylinositol 4,5-*bis*phosphate (PtdIns(4,5)P_2) is cleaved by phospholipase C (PLC). A better understanding of how DGKE deficiency impacts the endothelial lipid landscape is critical to developing a treatment for this condition.

Methods: We used orthogonal methods to compare the lipid levels in two novel models of *DGKE* deficiency to their respective controls: an immortalized human umbilical vein endothelial cell (iHUVEC) engineered with CRISPR/Cas9 and a blood outgrowth endothelial cell (BOEC) from an affected patient. Methods included mass spectrometry lipidomics, radiolabeling of phosphoinositides with [^{3}H]*myo*-inositol, and live-tracking of a transfected fluorescent PtdIns(4,5)P_2 biosensor.

Results: Unexpectedly, mass spectrometry lipidomics data revealed that high 38:4-DAG was not observed in the two *DGKE*-deficient models. Instead, a reduction in 38:4-PtdIns(4,5)P_2 was the major abnormality.These results were confirmed with the other two methods in *DGKE*-deficient iHUVEC.

Conclusion: Reduced 38:4-PtdIns(4,5)P_2—but not increased 38:4-DAG—is likely to be key to the pro-thrombotic phenotype exhibited by patients with *DGKE* aHUS.

TRANSLATIONAL STATEMENT

Mutations in *DGKE* cause a severe renal thrombotic microangiopathy that affects young children and leads to end-stage renal disease before adulthood. DGKE preferentially phosphorylates diacylglycerol to its corresponding phosphatidic acid (PA), which is then used to synthesize PtdIns(4,5)P_2 via the phosphatidylinositol cycle. Understanding the disease pathophysiology is necessary to develop a treatment to prevent this outcome. This paper describes how we applied mass spectrometry lipidomics to two novel models of *DGKE* deficiency to investigate how this defect impacts the levels of diacylglycerol, PA and related phosphoinositides in endothelia. Unexpectedly, our data show that the critical abnormality caused by *DGKE* deficiency is not high diacylglycerol, but rather low PtdIns(4,5)P_2. Restoring endothelial PtdIns(4,5)P_2 homeostasis may be the cornerstone to treat these patients.

INTRODUCTION

aHUS is a rare disease that causes renal failure because of thrombosis in kidney glomeruli.[1] Most genetic forms of aHUS are caused by mutations that lead to hyperactivation of the complement system.[2] We recently showed that loss-of-function mutations in *DGKE* cause a novel form of aHUS that does not respond to anti-complement therapy.[3] Typically, an infant with recurrent episodes of renal thrombosis, usually preceded by minor infections, develops end-stage renal disease within 10-20 years of diagnosis.[3, 4]

DGKE is a lipid kinase that phosphorylates DAG to PA; DAG is produced when PLC hydrolyzes PtdIns(4,5)P_2.[5] DGKE is unique amongst DGKs because its preferred substrate is 38:4-DAG, a form of DAG containing stearoyl (18:0) and arachidonoyl (20:4) moieties.[6–8] DGKE is highly expressed in glomerular podocytes and endothelial cells (ECs).[3] However, of these two cell types, only the latter actively regulates thrombosis.[9]

Based on its enzymatic mode of action, it is generally assumed that *DGKE* deficiency leads to accumulation of its substrate, DAG, and concomitant depletion of the reaction product, PA.[10] In that context, enhanced DAG-dependent signaling is deemed central to the pathophysiology of *DGKE* aHUS.[10] While this assumption is eminently reasonable, there are no studies assessing directly how DGKE deficiency impacts the levels of DAG, PA or other related phospholipids in ECs or kidney glomeruli. The high DAG hypothesis thus remains unproven.

To address this issue, we developed a mass spectrometry lipidomics approach to quantify all the relevant lipids from the same sample. We also engineered two novel experimental models of *DGKE* deficiency: *1) DGKE*$^{-/-}$ iHUVEC clones modified using Cas9 genome editing, and 2) BOEC derived from a patient with *DGKE* aHUS. Our results, which do not support the high DAG hypothesis but

instead point to more complex effects on phosphoinositide biosynthesis, will help guide the development of novel therapies for *DGKE* aHUS, while also providing a unique opportunity to study fatty acyl chain-specific lipid biology.

CONCISE METHODS

DGKE$^{-/-}$ immortalized HUVEC (iHUVEC)

We used Cas9 RNA-guided nuclease genome editing coupled with dual single-guide RNAs to generate an EC line devoid of DGKE activity. The cell line used is RF24, an immortalized cell line derived from HUVEC (a generous gift from Dr. Ingbord Klaassen, University of Amsterdam).[11, 12] We used dual Cas9 RNA-guided nuclease genome editing to trigger either a large (14 kb) deletion and/or small indels in the *DGKE* gene (**Supplemental Figure 1**).[13] This approach yielded three clones with bi-allelic loss-of-function variations by triggering either a macrodeletion within the DGKE gene and/or frameshift mutations. Three wild-type clones were also generated as controls. Cell from passage 4-12 were used for experiments. We used established protocols to measure DGKE mRNA by RT-qPCR[14, 15] and EC cell surface markers by flow cytometry (CD31, CD54, CD105 and CD144).[16] All cell lines were systematically tested for the presence of mycoplasma contamination every year with the MycoAlert PLUS Mycoplasma Detection Kit (cat# LT07-705, Lonza, Basel, CHE).

Human BOEC from a patient with DGKE aHUS

Patient-derived BOEC are complementary to the iHUVEC approach because these cells are not immortalized and they harbor homozygous missense *DGKE* mutations known to cause disease. We used the established protocol to generate BOEC from a patient with molecularly confirmed diagnosis of *DGKE* aHUS (BOEC*DGKE*) and an unrelated adult control subject (**Supplemental Figure 2**).[17] All participants signed an informed consent form detailing this procedure. BOECs from passages 4-12

were used for experiments. *DGKE* mRNA levels and EC cell surface markers were investigated as described for iHUVEC.

Mass Spectrometry-Based Lipidomics on EC lines

To normalize the lipidomics data, half of a dish with confluent ECs was processed to quantify protein concentration using the Pierce BCA Protein Assay Kit (Thermo Fisher Scientific) according to the manufacturer's protocol. The other half was used for acidic lipid extraction with TCA precipitation following an established protocol.[18] Lipid analytical internal standards for DAG, PtdIns, $PtdInsP_2$ and $PtdInsP_3$ were added to the TCA precipitates (all from Avanti Polar Lipids, Inc). Extracted lipids were dried under a stream of N_2 gas and then stored at -80°C. Prior to analysis, phosphate negative charges on phosphoinositides were neutralized by methylation.

Samples were analyzed with mass spectrometry in the multiple reaction monitoring mode, using electrospray and positive ion mode, as described.[18] Peak areas for acyl-chain specific lipid species and standards were quantified by integrating mass spectrometry curves as previously described.[18] Peak areas were normalized to total protein levels and to the peak area of the corresponding synthetic lipid standard to account for differential loss of samples during lipid extractions and methylation. For analysis of lipid species without a corresponding synthetic lipid standard, the values were normalized to total protein and expressed as normalized peak areas. It is important to note that our study is optimized to confidently assess the levels of 38:4-containing lipids. While levels for the other measurable lipid species are also provided, the level of confidence should be assumed to be lower because of multiple testing issues.

Measurement of Phosphoinositides (PtdIns) Using Radioactive ^{3}H-inositol Labelling

iHUVEC cells were grown as described above except that just before the cells reached confluence,

the growth medium was changed to an inositol-free EC medium with endothelial growth supplements (both products from ScienCell). The solution was supplemented with 75 mCi/mL myo-[2-^{3}H(N)] inositol (Perkin Elmer) and 5% dialyzed inositol-free FBS. After 24 hours, adherent cells were scraped and processed following a protocol recently described.[19, 20] Briefly, lipids were extracted after precipitation and de-acylation. ^{3}H-inositol loading was measured with flow scintillation (^{3}H window) before storage at -20°C until ready for further processing. Data for specific phosphatidylinositide species were obtained with high performance liquid chromatography (HPLC) followed by flow scintillation based on their known retention times as described.[19] For each species, we recorded the peak area (total counts), subtracted the background signal, and normalized the resulting data against the parental PtdIns species. Results are expressed as n-fold change in *DGKE*$^{-/-}$ compared to control.

Measuring PtdIns(4,5)P_2 Using Fluorescently Labelled Lipid Binding Probes

Near-confluent iHUVEC were transfected with plasmids encoding the fluorescent PtdIns(4,5)P_2 biosensor PH-PLCδ-GFP.[21] It encodes for the pleckstrin homology (PH) domain of phospholipase C delta (PLCδ) fused to GFP (gift from Dr S. Grinstein).[21] Cells were analyzed by confocal microscopy 24-48 hours post-transfection and after short exposure to the nuclear stain Hoechst® 33342 (Thermo Fisher Scientific). Data were captured and analyzed using Volocity Software (Perkin Elmer, Woodbridge, Canada). The mean GFP fluorescence intensity per pixel was measured in the plasma membrane (PM) and cytosol (cyt); background signal was subtracted from each value. The semi-quantitative measure of plasmalemmal PtdIns(4,5)P_2 was quantified as the ratio of PM/Cyt GFP fluorescence.

Statistical Analysis

All data represent three independent experiments unless otherwise indicated. Data is represented as

mean ± standard deviation, unless otherwise stated. All experiments were assessed using unpaired t-tests performed with Prism 7 (GraphPad Software, San Diego, CA).

RESULTS

Generation of a *DGKE*-deficient endothelial model

To better understand the pathogenesis of *DGKE* aHUS, we studied the impact of complete *DGKE* deficiency on the lipid profile of ECs. We focused our studies on these cells because they have an established role in regulating thrombosis, whereas podocytes do not.[22] To this end, we applied CRISPR/Cas9 to iHUVEC[11, 12] to generate three *DGKE*$^{-/-}$ clones (**Figure 1A-B**). *DGKE*$^{-/-}$ cells have reduced levels of *DGKE* mRNA and protein, are free of mutations at predicted off-target sites, have normal levels of EC surface markers by flow cytometry, and their wound healing ability is similar to that of control cells (**Supplemental Figure 1**).

DGKE-deficient iHUVEC have low PA

Since DGKE phosphorylates DAG to PA, the absence of a functional enzyme may be predicted to cause PA reduction (**Figure 1C**). We compared the lipid composition of wild-type and *DGKE*$^{-/-}$ iHUVECs by mass spectrometry to validate this prediction. The sum of all measurable PA species was significantly lower in *DGKE*$^{-/-}$ when compared to wild-type (**Figure 1D**). DGKE is known to preferentially phosphorylate DAG decorated with 38:4 fatty acyl chains –stearic acid, 18:0; arachidonic acid, 20:4– to the corresponding PA. A more detailed lipidomic analysis was therefore undertaken to investigate whether this PA species was particularly affected. As expected, we found that 38:4-PA levels were markedly reduced in *DGKE*$^{-/-}$ iHUVEC (**Figure 1E**). However, PAs decorated with other acyl chain combinations also appeared to be significantly lower in these cells (**Figure 1E**).

These data confirm that DGKE activity is indeed critical to generate 38:4-PA, a finding consistent

with earlier *in vitro* studies on the enzymatic activity of DGKE.[7, 8, 23, 24] Our results also suggest that the other nine mammalian DGKs –none of which have specificity for 38:4-DAG[25, 26]– cannot fully compensate for *DGKE* deficiency.

DAG is not elevated in *DGKE*$^{-/-}$ iHUVEC

The reduced formation of PA observed in the *DGKE*-deficient cells should, in principle, be accompanied by accumulation of its precursor, DAG (**Figure 1C**). Strikingly, we found the total DAG content to be markedly reduced in *DGKE*-deficient iHUVEC (**Figure 1F**). Detailed mass spectrometric analyses revealed that the decrease was most significant for 38:4-DAG, although other species were also depressed (**Figure 1G**). These unexpected results suggest that the cellular changes accompanying *DGKE* deficiency are more complex than anticipated.

Generation of patient-derived EC model of *DGKE* deficiency

The unexpected findings described above may reflect a peculiarity of gene-edited iHUVEC. It was therefore important to validate their occurrence in alternative experimental models of *DGKE* deficiency. Towards this goal, we generated BOEC[17] from a patient with a novel homozygous *DGKE* mutation (c.A494G; p.D165G; **Figures 2A-B**) and from an unrelated control. The aforementioned patient displayed classic features of *DGKE* aHUS (**Supplemental Figure 2A**). After confirming the genotypes of the BOEC*DGKE* (**Figure 2C**), we documented that when compared to controls, these cells have reduced levels of *DGKE* mRNA but similar levels of key EC surface markers (**Supplemental Figures 2B-C**).

38:4-PA is low and 38:4-DAG is not high in BOEC^{DGKE}

We used mass spectrometry to assess if PA reductions were also observed in BOEC*DGKE*. Detailed analysis of the discrete PA composition showed that these cells had significantly lower 38:4-

PA while having elevated levels for nearly all other PA species measured (**Figure 2D**). As a result, total PA was marginally higher when comparing mutant to control BOEC (**Figure 2E**).

We then sought to determine if the level of 38:4-DAG in BOEC*DGKE* would be elevated, conforming to the prediction (**Figure 1C**), or would instead replicate the unexpected results obtained with *DGKE*$^{-/-}$ iHUVEC (**Figure 1G**). Similar to the pattern observed for PA in BOEC*DGKE*, we found a trend towards lower 38:4-DAG (p=0.074) accompanied by significant increases in most other DAG species (**Figure 2F**). As a result, total DAG levels were significantly elevated in BOEC*DGKE* (**Figure 2G**).

Altogether, the parallel reductions in 38:4-PA and 38:4-DAG observed in BOEC*DGKE* resembles that observed with *DGKE*$^{-/-}$ iHUVEC, despite the fact that the total PA and DAG data are different between experimental models. The compensatory increases in PA and DAG noted in BOEC*DGKE*, which involved various species decorated with the same acyl chains, suggest the coordinated activation of enzyme sets that are unique to BOEC.

Low 38:4-PtdInsP$_2$ is a core feature of both *DGKE*-deficient experimental models

The reduced 38:4-PA levels observed in both models are attributable to the absence of DGKE activity, but must also be due in part to the reduced availability of its substrate, 38:4-DAG. The paucity of 38:4-DAG, while unexpected, may play an important role in the pathogenesis of *DGKE* aHUS. We therefore proceeded to investigate the mechanism underlying this paradoxical finding. Reduced 38:4-DAG could result from decreased 38:4-PtdInsP$_2$, its immediate precursor, to reduced phospholipase C activity, and/or to enhanced activity of other DAG metabolizing enzymes (**Supplemental Figure 3**). That low 38:4-PtdInsP$_2$ may be responsible for the abnormal DAG content is suggested by prior studies[8, 27] that ascribed to DGKE a key role in the phosphatidylinositol (PI) cycle; biosynthesis of

PtdIns, the precursor of $PtdInsP_2$, requires PA, which is in turn generated from DAG by DGK (**Figure 3A**).

We therefore compared the $PtdInsP_2$ content of wild-type versus *DGKE*-deficient cells by mass spectrometry, using the two systems described above. Total $PtdInsP_2$ measurements showed significant differences between wild-type and *DGKE*-deficient samples in both systems (**Figures 3B-D**). As was the case for total DAG, total $PtdInsP_2$ content was lower in the $DGKE^{-/-}$ iHUVEC when compared to wild-type samples. The situation was reversed for BOEC*DGKE*, with slightly higher $PtdInsP_2$ content, resembling the findings obtained for DAG (**Figure 2G**). The similarities between systems were greater when individual $PtdInsP_2$ species were analyzed. The content of 38:4-$PtdInsP_2$ was reduced in both models of *DGKE* deficiency (**Figures 3E-G**). Moreover, the net increase in $PtdInsP_2$ content recorded in BOEC*DGKE* was attributable to an elevation in $PtdInsP_2$ species with the same acyl chain combinations observed for PA and DAG.

Collectively, these results strongly suggest that, by reducing the availability of 38:4-PA, *DGKE* deficiency alters the PI cycle, preferentially affecting the synthesis of 38:4-$PtdInsP_2$, the most biologically active form of $PtdInsP_2$.[28]

Reduction in 38:4-$PtdInsP_2$ is due to low $PtdIns(4,5)P_2$

Mass spectrometric analyses can quantify the content of $PtdInsP_2$ with specific acyl chains but cannot distinguish among the three constituent isomers, namely $PtdIns(4,5)P_2$, $PtdIns(3,4)P_2$ and $PtdIns(3,5)P_2$. $PtdIns(4,5)P_2$ is generally more abundant than the two other species, and is therefore likely to account for the observed changes, but direct demonstration of this assumption was lacking. Two approaches were used to address this possibility. First we took advantage of the genetically-encoded biosensor PLCδ-PH-GFP that specifically binds to the headgroup of $PtdIns(4,5)P_2$.[21] When

expressed in iHUVEC, this probe partitions preferentially to the plasma membrane (**Figure 4A**), as described for other cell types.[21] The ratio of plasmalemmal-to-cytoplasmic GFP fluorescence was used as a measure of relative PtdIns(4,5)P_2 abundance, thereby accounting for differences in transfection efficiency between cells. When estimated in this fashion, the PtdIns(4,5)P_2 content of all 3 *DGKE*$^{-/-}$ iHUVEC clones was 20-30% lower than controls (**Figure 4B; Supplemental Figure 4**).

It is challenging to measure PtdIns(3,4)P_2 or PtdIns(3,5)P_2 using fluorescent lipid-binding probes because these species are comparatively scarce in cells.[29, 30] Furthermore, a high-avidity probe for PtdIns(3,4)P_2 was not available until very recently[31], and the validity of the only available probe for PtdIns(3,5)P_2[32] has been questioned.[33] To circumvent these problems, we attempted to fractionate the different PtdInsP_2 isomers by HPLC to resolve the relative abundance. Newly synthesized phosphoinositides were metabolically labeled with [^{3}H]*myo*-inositol after incubating confluent cells in inositol-free medium. Lipid extracts were deacylated and head-groups were separated by HPLC and detected by flow scintillation.

Because each experiment requires large amounts of [^{3}H]*myo*-inositol, only a single *DGKE*$^{-/-}$ iHUVEC clone (KO23) was compared with a control. We found that [^{3}H]*myo*-inositol uptake was similar between these cell. Reassuringly, newly synthesized PtdIns(4,5)P_2 levels were significantly decreased (by ≈20%) in *DGKE*$^{-/-}$ compared to control iHUVEC (**Figure 4B**). Of note, the sum of PtdIns(3,4)P_2 and PtdIns(3,5)P_2, which could not be independently resolved by the chromatographic scheme applied, was higher in *DGKE*$^{-/-}$ cells, although the increase did not attain statistical significance. This increase is unlikely to be of biological significance since the contribution of PtdIns(3,4)P_2 and PtdIns(3,5)P_2 to the total PtdInsP_2 pool is negligible. Indeed, despite the increase in these two species, the total PtdInsP_2 content –which is dominated by PtdIns(4,5)P_2– was lower in *DGKE*$^{-/-}$ compared to

control iHUVEC (**Figure 4C**).

Overall, the data from 3 orthogonal methods strongly suggest that at least in iHUVEC, *DGKE* deficiency causes a significant reduction in $PtdInsP_2$ levels that is mostly explained by abnormal $PtdIns(4,5)P_2$ metabolism. This phenomenon is attributable at least in part by changes in 38:4-$PtdIns(4,5)P_2$ and is seemingly accompanied by a small compensatory increase in $PtdIns(3,4)P_2$ and $PtdIns(3,5)P_2$ of unknown physiologic significance.

Impact of *DGKE* deficiency on $PtdIns(3,4,5)P_3$

Finally, we sought to determine if the reduced 38:4-$PtdInsP_2$ found in *DGKE*$^{-/-}$ iHUVEC translated into lower 38:4-$PtdIns(3,4,5)P_3$ levels. This would be an important finding because *DGKE* deficiency would then simultaneously affect two major signaling pathways: one dependent on PLC, and the other on phosphatidylinositol 3-kinase (PI3K**; Figure 5A**). We obtained robust and reproducible mass spectrometry lipidomics data even though $PtdIns(3,4,5)P_3$ is considerably less abundant than $PtdInsP_2$ in cells in basal state (not serum starved). We found that only 38:4-$PtdIns(3,4,5)P_3$ levels were significantly lower in *DGKE*$^{-/-}$ iHUVEC, compared to control cells (**Figure 5B**). None of the other species was significantly affected. Using the same approach, we also found trends towards lower 38:4-$PtdIns(3,4,5)P_3$ levels in BOEC*DGKE*, but this difference was not statistically significant (**Figure 5C**).

In *DGKE*$^{-/-}$ iHUVEC, the sum of all $PtdIns(3,4,5)P_3$ isomers was only marginally lower in *DGKE*-deficient cells (**Figure 5D**). However, the difference was significant when newly synthesized $PtdIns(3,4,5)P_3$ was assessed by HPLC analysis of cells radiolabelled with [^{3}H]*myo*-inositol (**Figure 5E**).This suggests that the pool of 38:4-$PtdIns(3,4,5)P_3$, and its precursor 38:4-$PtdIns(4,5)P_2$, turns over faster than other species. Taken together, these data suggest that reduced 38:4-$PtdIns(4,5)P_2$ content associated with *DGKE* deficiency causes a secondary reduction in 38:4-$PtdIns(3,4,5)P_3$ levels.

DISCUSSION

We often presume the root cause of *DGKE* aHUS to be excessive DAG-dependent signaling (e.g., via protein kinase C (PKC)).[10, 34] However, it is unclear if it elevates DAG in affected tissues of patients. Our findings are inconsistent with this notion. We showed that while 38:4-PA was low in *DGKE*-deficient cells, the content of 38:4-DAG was not increased concomitantly. We obtained similar results in two distinct experimental models of *DGKE* deficiency. Instead of the predicted DAG elevation, the salient and most consistent finding was the paucity of 38:4-PtdIns(4,5)P_2 (**Figures 3 & 4**). We, therefore, conclude that DGKE is essential for the generation 38:4-PA, which is itself required for the PI cycle to generate and maintain plasmalemmal 38:4-PtdIns(4,5)P_2 levels. We suggest that *DGKE* deficiency should be re-defined as an inborn error of phosphoinositide biogenesis.

The low levels of 38:4-PtdIns(4,5)P_2 are likely a direct consequence of reduced 38:4-PA, the critical substrate to initiate the PI cycle. Since 38:4-PtdIns(4,5)P_2 accounts for ~50-80% of PtdIns(4,5)P species in primary cells and fresh tissue[18, 35–37], it is likely central to many cellular processes, including signal transduction, membrane transport and actin cytoskeleton remodeling.[5] *In vivo*, these functions are carried out directly by 38:4-PtdIns(4,5)P_2, or indirectly via its hydrolysis to 38:4-DAG and Ins(1,4,5)P_3 by PLC, or by phosphorylation to 38:4-PtdIns(3,4,5)P_3 by PI3K.[5] While PLC and PI3K isoforms have no selectivity for PtdIns(4,5)P_2 species, 38:4-PtdIns(4,5)P_2 is their main substrate given its preponderance in cells. The remarkable phenotype associated with *DGKE* deficiency suggests that kidneys are uniquely sensitive to reduced levels of 38:4-PtdIns(4,5)P_2 or its products.

It is striking that low 38:4-PtdIns(4,5)P_2 is also the primary abnormality of cells deficient in other enzymes with 38:4 specificity, namely lysophosphatidylinositol-acyltransferase (LPIAT1)[38], lysocardiolipin acyltransferase (LYCAT)[19, 39] and CDP-DAG synthase 2 (CDS2).[40] Interestingly, CDS2 silencing in Zebrafish and HUVEC primarily disrupts endothelial functions.[41] While cells invest vast

resources to produce 38:4-PtdIns(4,5)P_2, little is known about the functional importance of various acyl chains. Studying *DGKE* deficiency provides a unique opportunity to investigate this question.

As stated above, *DGKE*-deficient ECs did not have high 38:4-DAG levels when compared to controls. This unexpected observation may be due to reduced PLCδ or PLCγ activation, two major PLC isoforms that are expressed in endothelial cells[42, 43] and use PtdIns(4,5)P_2 as their preferred substrate. The PH domain of PLCγ that is instrumental in its recruitment to the membrane, selectively binds PtdIns(3,4,5)P_3[44], which is depleted *pari passu* with PtdIns(4,5)P_2 in *DGKE*-deficient cells. The activation of PLCδ is similarly regulated, but via the binding of its PH domain to PtdIns(4,5)P_2 itself.[45, 46]

Given our results, it is prudent to re-interpret prior studies that assumed that elevated DAG is central to *DGKE* deficiency. The increased p38 and p44/42 activation observed earlier[34] following *DGKE* siRNA knockdown in HUVEC may not be attributable to high PKC activity. Accordingly, PKC activity was not increased in these cells.[34] In this context, it will be important to assess if *DGKE* silencing phenocopies *DGKE* knockout in terms of 38:4-PtdIns(4,5)P_2 levels, in which case the depletion of this phosphoinositide (or of a metabolite produced therefrom) may explain the altered activity of the two kinases. This is important because the phenotype of siRNA knockdown is not always concordant with that of a gene knockout.[47–49] Lastly, it is noteworthy that our results are in agreement with earlier studies that measured lipid levels in brain extracts[50] and fibroblast cell lines[23] derived from the original *Dgke*$^{-/-}$ and control mice. While we noted no differences in DAG levels, both reports highlighted the reduced PtdInsP_2.[23, 50]

That overexpressing DGKE in porcine aortic ECs triggered a reduction in 38:4-DAG[51] may at first appear to contradict our results. However, a likely explanation relates to the essentiality, in both

scenarios, of the physiological rate-limiting step of the PI cycle which, judging from our results, is the generation of 38:4-PtdIns(4,5)P_2. Excessive heterologous expression of DGKE should reduce the levels of its substrate DAG regardless of 38:4-PtdIns(4,5)P_2 levels. In contrast, *DGKE*-deficient cells are exquisitely sensitive to the rate-limiting step since 38:4-PtdIns(4,5)P_2 is in short supply.

Our findings show that therapies aimed at reducing DAG levels are unlikely to benefit patients with *DGKE* aHUS. We should instead focus efforts on restoring 38:4-PtdIns(4,5)P_2 levels, perhaps with intravenous infusion of the lipid itself or, more likely, of its more membrane-permeant precursors. This could mitigate the predicted effects on the actin cytoskeleton, the suboptimal anti-thrombotic protein levels (via defective exocytosis) or decreased nitric oxide production (via poor response to shear stress). Repurposing glycerol[52, 53] may be an attractive candidate therapy since its uptake and phosphorylation –two key steps in *de novo* PA synthesis[54]– are markedly increased in *Dgke*$^{-/-}$ cells.[55] The propensity of patients to develop renal thrombosis following minor infections[4] suggests that glomerular lipids help prevent excessive thromboinflammation.[56] Acute dampening of systemic inflammation with immunomodulatory agents could thus provide alternative treatment options.

ACKNOWLEDGMENTS

We thank Dr. Sergio Grinstein (Cell Biology Program, SickKids Research Institute) for helpful discussion and comments on the manuscript. VS was supported by the Frederick Banting and Charles Best Canada Graduate Scholarships (CGS-M) and the RESTRACOMP Master's Scholarship from the Hospital for Sick Children. RJB is funded by Natural Sciences and Engineering Research Council, Canada Research Chair Program, Early Researcher Award and Ryerson University. ML is supported by New Investigator Awards from KRESCENT/CHIR and CCHCSP. This research is funded by an operating grant from KRESCENT/CIHR.

DISCLOSURES

The authors have no conflict of interest to disclose.

REFERENCES

1. Noris M, Remuzzi G. Atypical hemolytic-uremic syndrome. *N Engl J Med*. 2009; 361: 1676-1687.

2. Noris M, Mescia F, Remuzzi G. STEC-HUS, atypical HUS and TTP are all diseases of complement activation. *Nat Rev Nephrol*. 2012; 8: 622-633.

3. Lemaire M, Frémeaux-Bacchi V, Schaefer F, Choi M, Tang WH, Le Quintrec M, Fakhouri F, Taque S, Nobili F, Martinez F, Ji W, Overton JD, Mane SM, Nürnberg G, Altmüller J, Thiele H, Morin D, Deschenes G, Baudouin V, Llanas B, Collard L, Majid MA, Simkova E, Nürnberg P, Rioux-Leclerc N, Moeckel GW, Gubler MC, Hwa J, Loirat C, Lifton RP. Recessive mutations in DGKE cause atypical hemolytic-uremic syndrome. *Nat Genet*. 2013; 45: 531-536.

4. Azukaitis K, Simkova E, Majid MA, Galiano M, Benz K, Amann K, Bockmeyer C, Gajjar R, Meyers KE, Cheong HI, Lange-Sperandio B, Jungraithmayr T, Frémeaux-Bacchi V, Bergmann C, Bereczki C, Miklaszewska M, Csuka D, Prohászka Z, Gipson P, Sampson MG, Lemaire M, Schaefer F. The Phenotypic Spectrum of Nephropathies Associated with Mutations in Diacylglycerol Kinase ε. *J Am Soc Nephrol*. 2017; 28: 3066-3075.

5. Epand RM, So V, Jennings W, Khadka B, Gupta RS, Lemaire M. Diacylglycerol Kinase-ε: Properties and Biological Roles. *Front Cell Dev Biol*. 2016; 4: 112.

6. Lung M, Shulga YV, Ivanova PT, Myers DS, Milne SB, Brown HA, Topham MK, Epand RM. Diacylglycerol kinase epsilon is selective for both acyl chains of phosphatidic acid or diacylglycerol. *J Biol Chem*. 2009; 284: 31062-31073.

7. Shulga YV, Topham MK, Epand RM. Substrate specificity of diacylglycerol kinase-epsilon and the phosphatidylinositol cycle. *FEBS Lett*. 2011; 585: 4025-4028.

8. Shulga YV, Topham MK, Epand RM. Study of arachidonoyl specificity in two enzymes of the PI cycle. *J Mol Biol*. 2011; 409: 101-112.

9. Yau JW, Teoh H, Verma S. Endothelial cell control of thrombosis. *BMC Cardiovasc Disord*. 2015; 15: 130.

10. Quaggin SE. DGKE and atypical HUS. *Nat Genet*. 2013; 45: 475-476.

11. Fontijn R, Hop C, Brinkman HJ, Slater R, Westerveld A, van Mourik JA, Pannekoek H. Maintenance of vascular endothelial cell-specific properties after immortalization with an

amphotrophic replication-deficient retrovirus containing human papilloma virus 16 E6/E7 DNA. *Exp Cell Res*. 1995; 216: 199-207.

12. Ades EW, Candal FJ, Swerlick RA, George VG, Summers S, Bosse DC, Lawley TJ. HMEC-1: establishment of an immortalized human microvascular endothelial cell line. *J Invest Dermatol*. 1992; 99: 683-690.

13. Ye L, Wang J, Tan Y, Beyer AI, Xie F, Muench MO, Kan YW. Genome editing using CRISPR-Cas9 to create the HPFH genotype in HSPCs: An approach for treating sickle cell disease and β-thalassemia. *Proc Natl Acad Sci USA*. 2016; 113: 10661-10665.

14. Livak KJ, Schmittgen TD. Analysis of relative gene expression data using real-time quantitative PCR and the 2(-Delta Delta C(T)) Method. *Methods*. 2001; 25: 402-408.

15. Wu J, Duan R, Cao H, Field D, Newnham CM, Koehler DR, Zamel N, Pritchard MA, Hertzog P, Post M, Tanswell AK, Hu J. Regulation of epithelium-specific Ets-like factors ESE-1 and ESE-3 in airway epithelial cells: potential roles in airway inflammation. *Cell Research*. 2008; 18: 649-663.

16. Reiss Y, Engelhardt B. FACS analysis of endothelial cells. *Methods in Endothelial Cell Biology*. 2004; 157-165.

17. Martin-Ramirez J, Hofman M, van den Biggelaar M, Hebbel RP, Voorberg J. Establishment of outgrowth endothelial cells from peripheral blood. *Nat Protoc*. 2012; 7: 1709-1715.

18. Traynor-Kaplan A, Kruse M, Dickson EJ, Dai G, Vivas O, Yu H, Whittington D, Hille B. Fatty-acyl chain profiles of cellular phosphoinositides. *Biochim Biophys Acta Mol Cell Biol Lipids*. 2017; 1862: 513-522.

19. Bone LN, Dayam RM, Lee M, Kono N, Fairn GD, Arai H, Botelho RJ, Antonescu CN. The acyltransferase LYCAT controls specific phosphoinositides and related membrane traffic. *Mol Biol Cell*. 2017; 28: 161-172.

20. Ho CY, Choy CH, Botelho RJ. Radiolabeling and Quantification of Cellular Levels of Phosphoinositides by High Performance Liquid Chromatography-coupled Flow Scintillation. *J Vis Exp*. 2016; 125-131.

21. Várnai P, Balla T. Visualization of phosphoinositides that bind pleckstrin homology domains: calcium- and agonist-induced dynamic changes and relationship to myo-[3H]inositol-labeled phosphoinositide pools. *J Cell Biol*. 1998; 143: 501-510.

22. Roumenina LT, Rayes J, Frimat M, Fremeaux-Bacchi V. Endothelial cells: source, barrier, and

target of defensive mediators. *Immunol Rev*. 2016; 274: 307-329.

23. Milne SB, Ivanova PT, Armstrong MD, Myers DS, Lubarda J, Shulga YV, Topham MK, Brown HA, Epand RM. Dramatic differences in the roles in lipid metabolism of two isoforms of diacylglycerol kinase. *Biochemistry*. 2008; 47: 9372-9379.

24. Benigni A, Corna D, Zoja C, Sonzogni A, Latini R, Salio M, Conti S, Rottoli D, Longaretti L, Cassis P, Morigi M, Coffman TM, Remuzzi G. Disruption of the Ang II type 1 receptor promotes longevity in mice. *J Clin Invest*. 2009; 119: 524-530.

25. Sakai H, Kado S, Taketomi A, Sakane F. Diacylglycerol kinase δ phosphorylates phosphatidylcholine-specific phospholipase C-dependent, palmitic acid-containing diacylglycerol species in response to high glucose levels. *J Biol Chem*. 2014; 289: 26607-26617.

26. Sakane F, Mizuno S, Takahashi D, Sakai H. Where do substrates of diacylglycerol kinases come from? Diacylglycerol kinases utilize diacylglycerol species supplied from phosphatidylinositol turnover-independent pathways. *Adv Biol Regul*. 2018; 67: 101-108.

27. Shulga YV, Myers DS, Ivanova PT, Milne SB, Brown HA, Topham MK, Epand RM. Molecular species of phosphatidylinositol-cycle intermediates in the endoplasmic reticulum and plasma membrane. *Biochemistry*. 2010; 49: 312-317.

28. Epand RM. Features of the Phosphatidylinositol Cycle and its Role in Signal Transduction. *J Membr Biol*. 2017; 250: 353-366.

29. Li H, Marshall AJ. Phosphatidylinositol (3,4) bisphosphate-specific phosphatases and effector proteins: A distinct branch of PI3K signaling. *Cell Signal*. 2015; 27: 1789-1798.

30. McCartney AJ, Zhang Y, Weisman LS. Phosphatidylinositol 3,5-bisphosphate: low abundance, high significance. *Bioessays*. 2014; 36: 52-64.

31. Goulden BD, Pacheco J, Dull A, Zewe JP, Deiters A, Hammond GRV. A high-avidity biosensor reveals plasma membrane PI(3,4)P2 is predominantly a class I PI3K signaling product. *J Cell Biol*. 2019; 218: 1066-1079.

32. Li X, Wang X, Zhang X, Zhao M, Tsang WL, Zhang Y, Yau RG, Weisman LS, Xu H. Genetically encoded fluorescent probe to visualize intracellular phosphatidylinositol 3,5-bisphosphate localization and dynamics. *Proc Natl Acad Sci U S A*. 2013; 110: 21165-21170.

33. Hammond GR, Takasuga S, Sasaki T, Balla T. The ML1Nx2 Phosphatidylinositol 3,5-Bisphosphate Probe Shows Poor Selectivity in Cells. *PLoS One*. 2015; 10: e0139957.

34. Bruneau S, Néel M, Roumenina LT, Frimat M, Laurent L, Frémeaux-Bacchi V, Fakhouri F. Loss of DGKε induces endothelial cell activation and death independently of complement activation. *Blood*. 2015; 125: 1038-1046.

35. Wenk MR, Lucast L, Di Paolo G, Romanelli AJ, Suchy SF, Nussbaum RL, Cline GW, Shulman GI, McMurray W, De Camilli P. Phosphoinositide profiling in complex lipid mixtures using electrospray ionization mass spectrometry. *Nat Biotechnol*. 2003; 21: 813-817.

36. Haag M, Schmidt A, Sachsenheimer T, Brügger B. Quantification of Signaling Lipids by Nano-Electrospray Ionization Tandem Mass Spectrometry (Nano-ESI MS/MS). *Metabolites*. 2012; 2: 57-76.

37. Hicks AM, DeLong CJ, Thomas MJ, Samuel M, Cui Z. Unique molecular signatures of glycerophospholipid species in different rat tissues analyzed by tandem mass spectrometry. *Biochim Biophys Acta*. 2006; 1761: 1022-1029.

38. Anderson KE, Kielkowska A, Durrant TN, Juvin V, Clark J, Stephens LR, Hawkins PT. Lysophosphatidylinositol-acyltransferase-1 (LPIAT1) is required to maintain physiological levels of PtdIns and PtdInsP(2) in the mouse. *PLoS One*. 2013; 8: e58425.

39. Imae R, Inoue T, Nakasaki Y, Uchida Y, Ohba Y, Kono N, Nakanishi H, Sasaki T, Mitani S, Arai H. LYCAT, a homologue of C. elegans acl-8, acl-9, and acl-10, determines the fatty acid composition of phosphatidylinositol in mice. *J Lipid Res*. 2012; 53: 335-347.

40. D'Souza K, Kim YJ, Balla T, Epand RM. Distinct properties of the two isoforms of CDP-diacylglycerol synthase. *Biochemistry*. 2014; 53: 7358-7367.

41. Pan W, Pham VN, Stratman AN, Castranova D, Kamei M, Kidd KR, Lo BD, Shaw KM, Torres-Vazquez J, Mikelis CM, Gutkind JS, Davis GE, Weinstein BM. CDP-diacylglycerol synthetase-controlled phosphoinositide availability limits VEGFA signaling and vascular morphogenesis. *Blood*. 2012; 120: 489-498.

42. Béziau DM, Toussaint F, Blanchette A, Dayeh NR, Charbel C, Tardif JC, Dupuis J, Ledoux J. Expression of phosphoinositide-specific phospholipase C isoforms in native endothelial cells. *PLoS One*. 2015; 10: e0123769.

43. Lo Vasco VR, Pacini L, Di Raimo T, D'arcangelo D, Businaro R. Expression of phosphoinositide-specific phospholipase C isoforms in human umbilical vein endothelial cells. *J Clin Pathol*. 2011; 64: 911-915.

44. Falasca M, Logan SK, Lehto VP, Baccante G, Lemmon MA, Schlessinger J. Activation of

phospholipase C gamma by PI 3-kinase-induced PH domain-mediated membrane targeting. *EMBO J*. 1998; 17: 414-422.

45. Lomasney JW, Cheng HF, Roffler SR, King K. Activation of phospholipase C delta1 through C2 domain by a Ca(2+)-enzyme-phosphatidylserine ternary complex. *J Biol Chem*. 1999; 274: 21995-22001.

46. Yagisawa H, Sakuma K, Paterson HF, Cheung R, Allen V, Hirata H, Watanabe Y, Hirata M, Williams RL, Katan M. Replacements of single basic amino acids in the pleckstrin homology domain of phospholipase C-delta1 alter the ligand binding, phospholipase activity, and interaction with the plasma membrane. *J Biol Chem*. 1998; 273: 417-424.

47. El-Brolosy MA, Stainier DYR. Genetic compensation: A phenomenon in search of mechanisms. *PLoS Genet*. 2017; 13: e1006780.

48. Rossi A, Kontarakis Z, Gerri C, Nolte H, Hölper S, Krüger M, Stainier DY. Genetic compensation induced by deleterious mutations but not gene knockdowns. *Nature*. 2015; 524: 230-233.

49. Dawlaty MM, Ganz K, Powell BE, Hu YC, Markoulaki S, Cheng AW, Gao Q, Kim J, Choi SW, Page DC, Jaenisch R. Tet1 is dispensable for maintaining pluripotency and its loss is compatible with embryonic and postnatal development. *Cell Stem Cell*. 2011; 9: 166-175.

50. Rodriguez de Turco EB, Tang W, Topham MK, Sakane F, Marcheselli VL, Chen C, Taketomi A, Prescott SM, Bazan NG. Diacylglycerol kinase epsilon regulates seizure susceptibility and long-term potentiation through arachidonoyl- inositol lipid signaling. *Proc Natl Acad Sci U S A*. 2001; 98: 4740-4745.

51. Pettitt TR, Wakelam MJ. Diacylglycerol kinase epsilon, but not zeta, selectively removes polyunsaturated diacylglycerol, inducing altered protein kinase C distribution in vivo. *J Biol Chem*. 1999; 274: 36181-36186.

52. Bayer AJ, Pathy MS, Newcombe R. Double-blind randomised trial of intravenous glycerol in acute stroke. *Lancet*. 1987; 1: 405-408.

53. Buckell M, Walsh L. Effect Of Glycerol By Mouth On Raised Intracranial Pressure In Man. *Lancet*. 1964; 2: 1151-1152.

54. Athenstaedt K, Daum G. Phosphatidic acid, a key intermediate in lipid metabolism. *Eur J Biochem*. 1999; 266: 1-16.

55. So V, Jalan D, Lemaire M, Topham MK, Hatch GM, Epand RM. Diacylglycerol kinase epsilon

suppresses expression of p53 and glycerol kinase in mouse embryo fibroblasts. *Biochim Biophys Acta*. 2016; 1861: 1993-1999.

56. Jackson SP, Darbousset R, Schoenwaelder SM. Thromboinflammation: Challenges of Therapeutically Targeting Coagulation and other Host Defence Mechanisms. *Blood*. 2019;

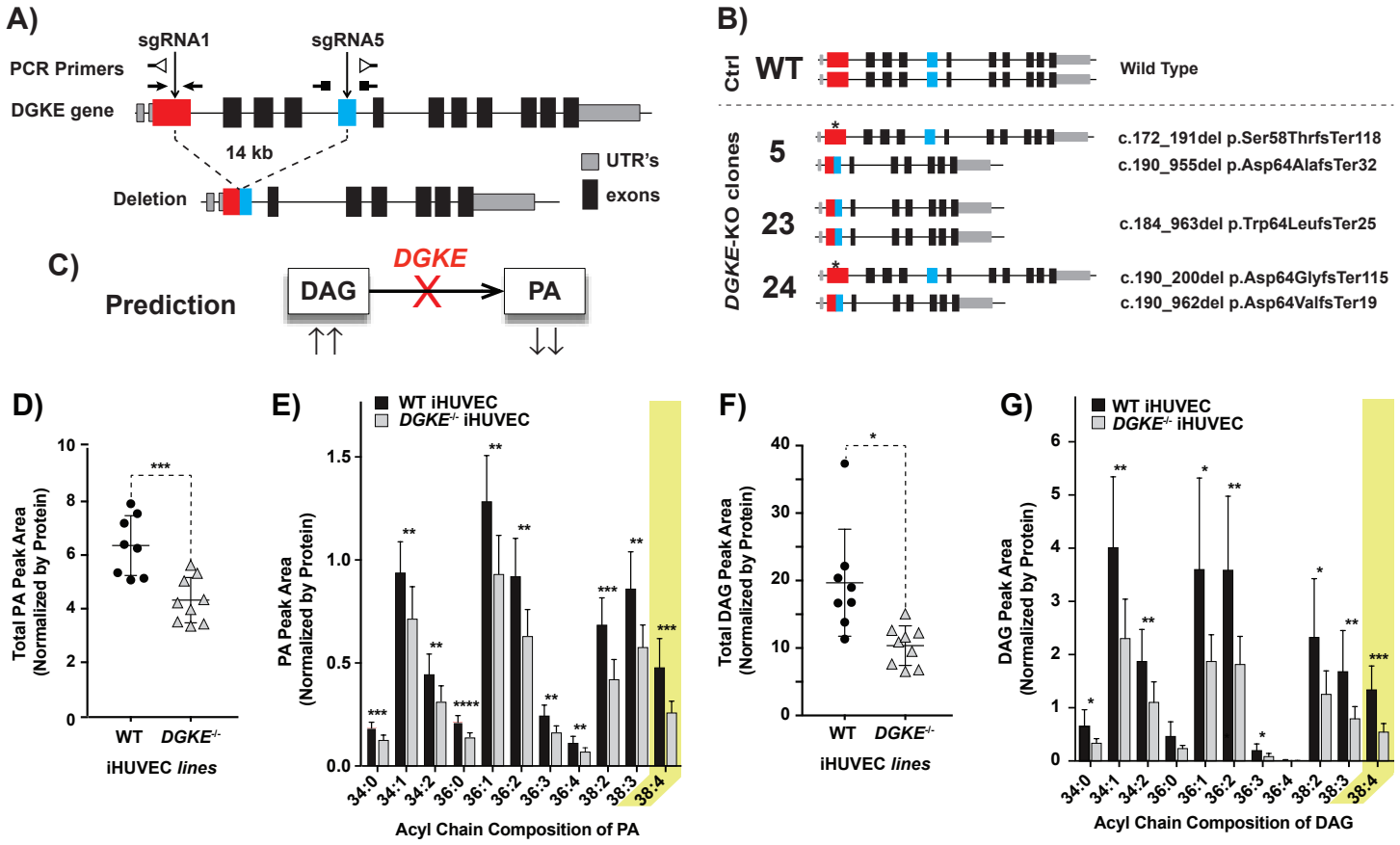

Figure 1: Immortalized *DGKE*$^{-/-}$ iHUVECs have reduced 38:4-PA and 38:4-DAG.

A) Strategy to generate *DGKE*$^{-/-}$ endothelial cell lines from immortalized HUVEC (iHUVEC; also known as RF24 cell lines). The relative positions of the sgRNAs used to generate a 14 kilobases (kb) macrodeletion (or small indel) by targeting exons 2 (red) and 6 (blue) within the human *DGKE* gene. The position of the oligonucleotide primers used to amplify the various segments are indicated: closed arrowheads indicate amplifications over short distances (small indels) and open head arrowheads indicate amplification over long segments (macrodeletions).

B) The genomic structure and the nucleotide sequences for each *DGKE*$^{-/-}$ clone, derived from PCR and Sanger sequencing. * indicates site where a small indel was created that induces a frameshift.

C) Illustration of the enzymatic reaction catalyzed by diacylglycerol kinase epsilon (DGKE).

D-G) *DGKE*$^{-/-}$ iHUVEC samples analyzed using mass spectrometry lipidomics to derive the sum total of all measurable PAs (D), the levels for each distinct measurable PA species (E), the sum total of all measurable DAGs (F), the levels for each distinct measurable DAG species (G). Lipids were precipitated from confluent monolayers of *DGKE*$^{-/-}$ or control iHUVEC and used in lipid extractions and methylation, coupled to mass spectrometry-based lipidomics for the endogenous detection of PA and DAG. All experiments were done with cells at steady-state (i.e., not stimulated nor starved). Bars represent the mean levels of each DAG and PA lipid species from at least three independent experiments for each of the three wild-type and 3 *DGKE*$^{-/-}$ clones (6 cell lines in total, and 17 independent measurements). The yellow colored rectangle indicate the values for our main target lipid, 38:4-PA and 38:4-DAG. Error bars represent standard deviation of the mean. * denotes $p<0.05$, ** $p<0.01$, *** $p<0.001$ and **** $p<0.0001$.

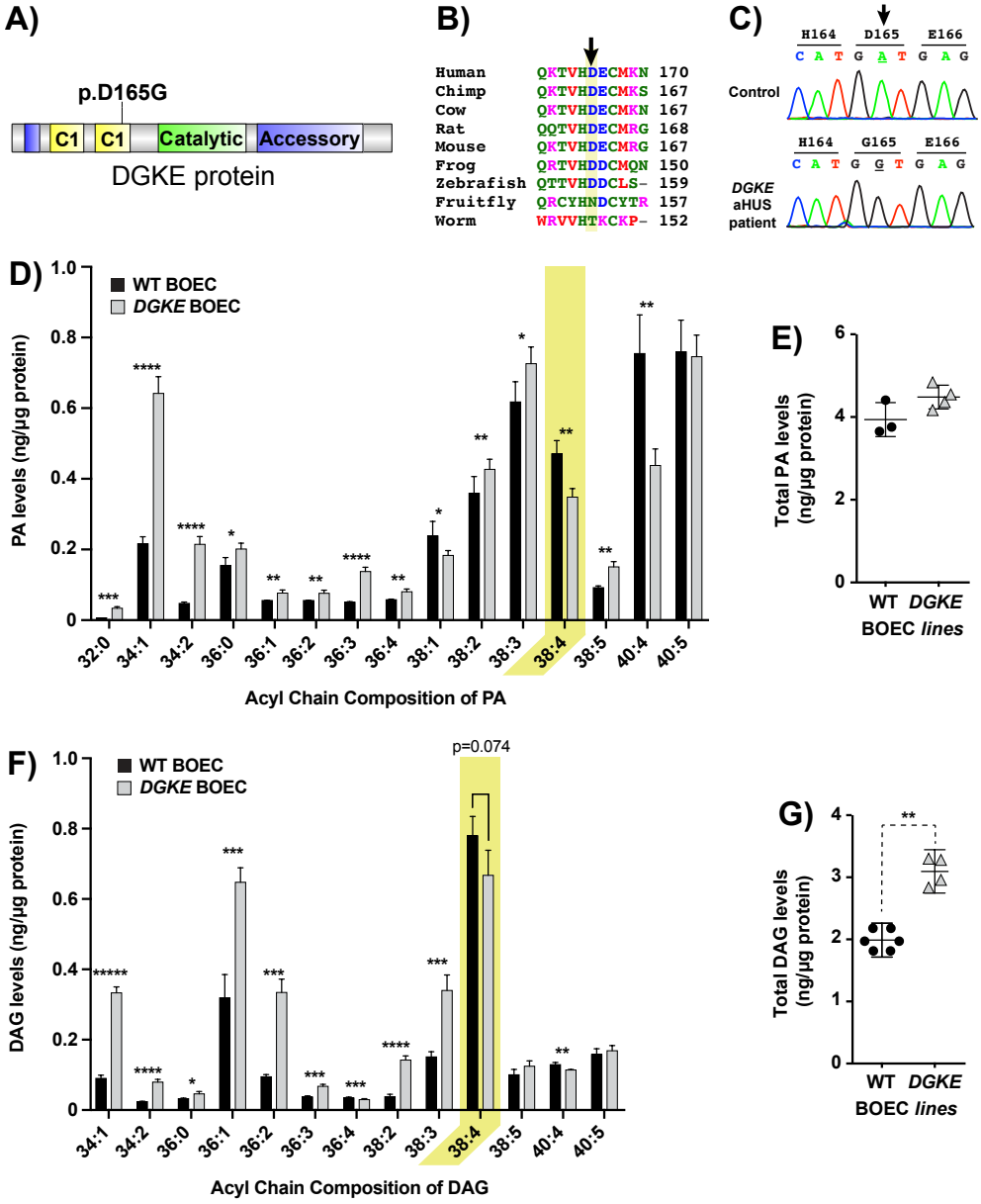

Figure 2: Blood outgrowth endothelial cells (BOEC) from a patient with *DGKE* aHUS have reduced 38:4-PA and 38:4-DAG.

A) Illustration of the functional domain of DGKE protein, with the relative position of the missense mutations found in the patient, located in the second C1 domain.

B) Alignment of the amino acid sequence of DGKE proteins from a variety of species showing that it is well-conserved down to the zebra fish.

C) DNA chromatograms showing the homozygous mutation found in the BOEC derived from the patient sample, c.A494G; p.D165G. Also shown is the sequence amplified from the same genomic segment of control BOEC.

D-G) *DGKE* BOEC samples analyzed using mass spectrometry lipidomics to derive the levels for each distinct measurable species of PA (D) or DAG (F) and the sum total of all measurable PAs (E) or DAGs (G). The same protocol described for iHUVEC was used. Bars represent the mean levels of each PA and DAG lipid species from 4 separate experiments with *DGKE* BOEC and 3 with control BOEC. The yellow colored rectangle indicate the values for our main target lipid, 38:4-PA and 38:4-DAG. Error bars represent standard deviation of the mean. * denotes $p<0.05$, ** $p<0.01$, *** $p<0.001$, **** $p<0.0001$ and ***** $p<0.00001$.

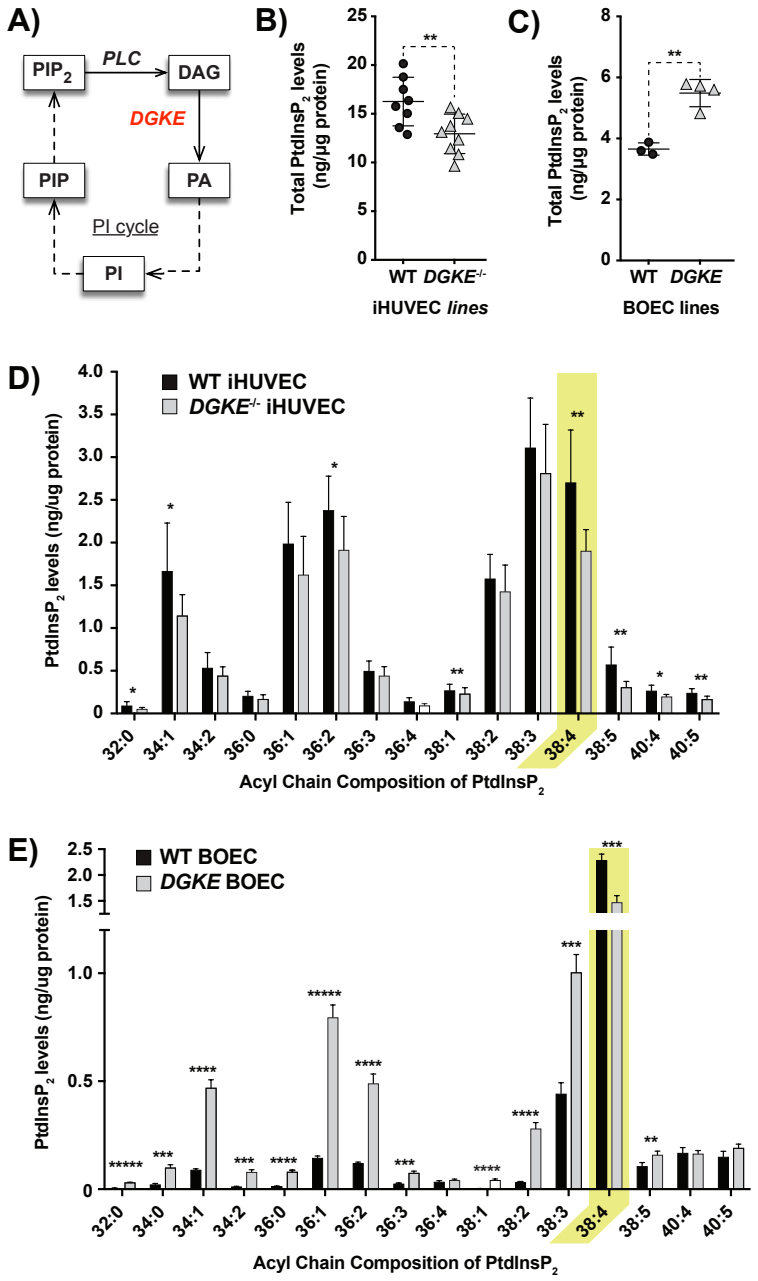

Figure 3: Both experimental models of DGKE deficiency all have reduced 38:4-PIP$_2$ levels.
A) Illustration of the major enzymes (phospholipase C (PLC) and DGKE) and lipids (PI, PIP, PIP$_2$, DAG and PA) implicated in the phosphoinositide (PI) cycle.
B-C) The sum total of all measurable PIP$_2$ for experiments done with iHUVEC (B) or BOEC (C). Wild-type and *DGKE*-deficient model systems are represented by "△" and "●", respectively.
D-E) The levels for each distinct measurable species of PIP$_2$ for experiments done with iHUVEC (D) or BOEC (E). Wild-type and *DGKE*$^{-/-}$ model systems are represented by black and white bars, respectively. The same protocol described for iHUVEC was used except that an internal PIP$_2$ standard decorated with 17:0/17:0 was used to improve the reliability of the semi-quantitative measurements. Bars represent the mean levels of each PIP$_2$ lipid species from at least three independent experiments (for details on the number of experiments for each model, please refer to Figures 1-3). The yellow colored rectangle indicate the values for the main target lipid, 38:4-PIP$_2$. Error bars represent standard deviation of the mean. * denotes $p<0.05$, ** $p<0.01$, *** $p<0.001$, **** $p<0.0001$ and ***** $p<0.00001$.

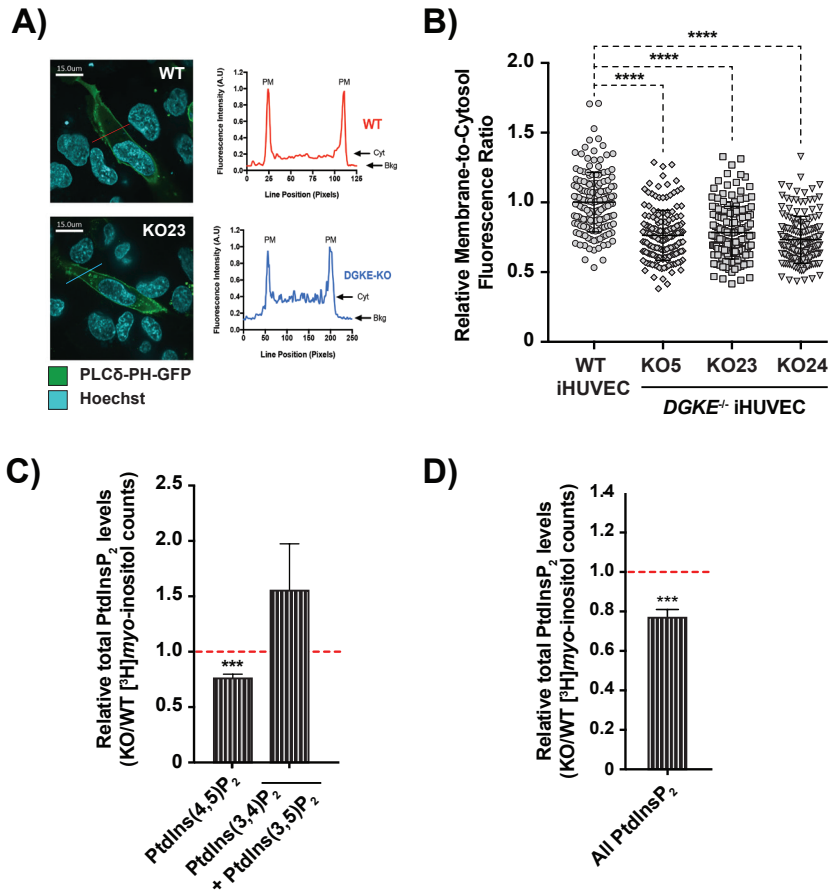

Figure 4: Low 38:4-PtdInsP$_2$ is caused by reduced PtdIns(4,5)P$_2$ levels in *DGKE*$^{-/-}$ iHUVEC.

A) Representative images of cells transfected with GFP-tagged PLCδ-PH lipid binding probe from WT iHUVEC cell line and DGKE-KO iHUVEC (clones KO5, KO23, and KO24). The KO23 clone is displayed as the representative image. Images are representative of 3 independent experiments. Next to each representative image is a line scan plot corresponding to the line drawn across the cell bodies (red for WT, and blue for KO23). The fluorescence intensity in arbitrary units (AU) was normalized to the highest fluorescence value.

B) Estimation of the relative levels of plasma membrane PtdIns(4,5)P$_2$ after transfection of iHUVEC with a fluorescent PtdIns (4,5)P$_2$ biosensor (PLCδ-PH-GFP). The ratio of plasma membrane fluorescence-to-cytoplasm (PM/Cyt) fluorescence was measured for at least 50 cells in three separate experiments for wild-type or *DGKE*$^{-/-}$ iHUVEC. Data represent the mean from aggregated data of at least 150 cells per clone, each point being the value of one cell. The ratio was normalized to the average ratio of PM/Cyt fluorescence across three experiments with wild-type cells. Error bars denote standard deviations. Unpaired t-tests were performed to compare wild-type cells to each knockout clone (KO5, KO23, KO24).

C) Relative levels of PtdInsP$_2$ isomers using [^{3}H]*myo*-inositol metabolic cell labeling followed by liquid scintillation counting of the HPLC eluent. All PtdInsP$_2$ species measurements were normalized to total PI levels. Values of *DGKE*$^{-/-}$ iHUVEC are expressed as radioactive counts relative to control iHUVEC counts. The dotted red line indicates the expected values if *DGKE*$^{-/-}$ iHUVEC have levels similar to control cells.

D) "All PtdInsP$_2$" data are derived from the sum of radioactive signals of PtdIns(3,4)P$_2$, PtdIns(3,5)P$_2$ and PtdIns(4,5)P$_2$. Data represent the mean of 3 independent experiments. The error bars denote standard deviation of the mean.

* denotes $p<0.05$, *** $p<0.001$ and **** $p<0.0001$.

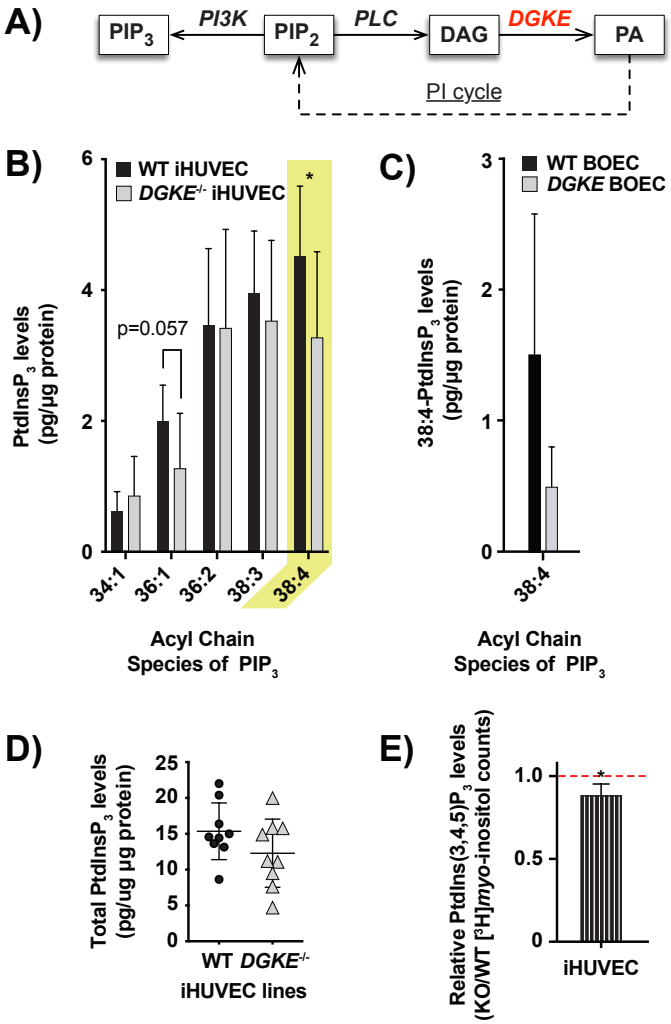

Figure 5: PtdInsP$_3$ data for both experimental models of *DGKE* deficiency: measurements by lipidomics and radioactive inositol labeling.

A) The pathways responsible for metabolizing PtdIns(4,5)P$_2$ to the two main bioactive metabolites, DAG and PtdIns(3,4,5)P$_3$. The PI cycle, which is responsible for synthesizing PtdIns(4,5)P$_2$ from PA, is also illustrated.

B-C) The levels for each distinct measurable species of PtdInsP$_3$ for experiments done with iHUVEC (B) or BOEC (C), analyzed using mass spectrometry lipidomics. The yellow colored rectangle indicate the values for the main target lipid, 38:4-PtdInsP$_3$. An internal PtdInsP$_3$ standard decorated with 17:0/17:0 was used to improve the reliability of the semi-quantitative measurements. Bars represent the mean levels of each PtdInsP$_3$ lipid species from at least three independent experiments (for details on the number of experiments for each model, please refer to Figures 1-3).

D) The sum total of all measurable PtdInsP$_3$ for mass spectrometry lipidomics experiments done with iHUVEC (p=0.157).

E) Relative levels of PtdIns(3,4,5)P$_3$ using [^{3}H]*myo*-inositol metabolic cell labeling followed by liquid scintillation counting of the HPLC eluent as described for PtdInsP$_2$ isomers. PtdIns(3,4,5)P$_3$ measurements were normalized to total PI levels. Values of *DGKE*$^{-/-}$ iHUVEC are expressed as radioactive counts relative to control iHUVEC counts. The dotted red line indicates the expected values if *DGKE*$^{-/-}$ iHUVEC have levels similar to control cells.

Error bars represent standard deviation of the mean. * denotes p<0.05.